Acta Acustica 2022, **6**, 12

https://doi.org/10.1051/aacus/2021058

Available online at:
https://acta-acustica.edpsciences.org

SCIENTIFIC ARTICLE OPEN ACCESS

2D phononic-crystal Luneburg lens for all-angle underwater sound localization

Yongdu Ruan (阮永都)[1,2] and Xu Liang (梁旭)[1,*]

[1] Ocean College, Zhejiang University, Zhoushan, Zhejiang 316021, PR China
[2] Research Center for Intelligent Sensing, Zhejiang Lab, Hangzhou, Zhejiang 311121, PR China

Received 6 September 2021, Accepted 16 December 2021

Abstract – Phononic crystals are well known for acoustic wave manipulation which may have potential application in an underwater acoustic detection system. In this work, we design and simulate a two-dimensional Luneburg lens based on gradient-index (GRIN) phononic crystal that is composed of PLA-Air inclusion, and a novel application of GRIN phononic crystals is proposed to sound localization. The Luneburg lens has a broadband working range, from 1500 Hz to 7500 Hz, for acoustic wave focusing with sensitive directivity and signal-to-noise improvement. By searching maximum wave intensity's position of the focusing beam, the propagating direction of an unknown sound wave can be directly recognized covering 360°. Besides, we redesign the conventional square-lattice Luneburg lenses using annular lattices for better performance. The annular-lattice Luneburg lens overcomes the weakness of configuration defect due to the square lattice. The numerical results show that the redesign Luneburg lenses have high accuracy for distance measurement from 5 m to 35 m through the triangulation location. In a word, this work tries to explore a novel application of phononic crystals in underwater acoustic positioning and navigation technology.

Keywords: Underwater metamaterials, Phononic crystal, Luneburg lens, Acoustic detection, Sound localization

1 Introduction

Recently, underwater acoustic metamaterial [1–5] attracts a lot of attention because its function of wave manipulation has potential applications in underwater technology, and a new crossing field may come out. As an initial version of acoustic metamaterial, the phononic crystal that is a periodic structure made of multiple mediums or a single-phase artificial microstructure enables negative refraction [6], wave bending [7], and splitting [8] to be realized. Due to the excellent performance of waveguide, phononic crystal is used for acoustic wave focusing [9–11], and the fabricated device is always named phononic-crystal lens. Acoustic Luneburg lens [12–15] is a gradient refraction index lens that can converge wave energy even though the acoustic wave enters from different directions covering 360°. This feature has great advantages for detecting an object which produces sound waves in a water environment, like underwater beacons and underwater vehicles. However, the conventional Luneburg lens is difficult to manufacture because the refractive index profile is not a uniform distribution [16] until the gradient-index (GRIN) phononic crystal [17] appears.

The design of a Luneburg lens lies in the arrangement of unit cells according to the discretized refraction index profile. In order to realize the effect of acoustic wave convergence, Kim et al. [13, 18] and Xie et al. [12] designed 2D and 3D Luneburg lenses based on the filling ratio of scatterer which is a function of effective refraction index, and Kim et al. [19] firstly utilized the discretized Luneburg lens for signal amplification in the ocean. Since the effective velocity of a periodic structure is proposed to be calculated based on the band structure [17], the phononic crystals as a more efficient and precise way than the filling ratio is used to design the Luneburg lens [15]. When the working environment is air, the fluid-solid coupling is always ignored [20, 21], so Yu et al. [22] redesigned an underwater Luneburg lens for enhancing the focused signal at a center frequency of 180 kHz. Allam et al. [23] and Lu et al. [24] provided a 3D-printed approach to replace the metallic structure for acoustic wave focusing using the Luneburg lens [25]. 3D-printed is the fastest way to fabricate the Luneburg lens if the hydrostatic pressure is ignored. For better performance, Sun et al. [26, 27] offered an optimized method to design the acoustic lens in the water environment. These researches lay a foundation for the application of phononic-crystal Luneburg lens in ocean technology and engineering.

*Corresponding author: Liangxu@zju.edu.cn

Finding an unknown sound in the ocean is difficult for human beings. The traditional approach for localizing a sound source is hydrophone arrays according to the time difference of receiving signal [28, 29]. To overcome that the accuracy of sound localization is limited by the number of the microphones and the array scale [30], researchers attempt to use the metamaterial to develop new sound localization techniques for more application scenarios [31, 32]. In this work, we designed square-lattice and annular-lattice Luneburg lenses based on GRIN phononic crystals whose unit cell is made of PLA and air inclusion in a water environment, and we proposed a novel application of GRIN phononic crystals to sound direction identification and sound localization covering 360°. The frequency response, sound directivity and sound amplification of the Luneburg lens within a range of 1500–7500 Hz are all studied, and the distance measurement via triangulation location is simulated from 5 m to 35 m.

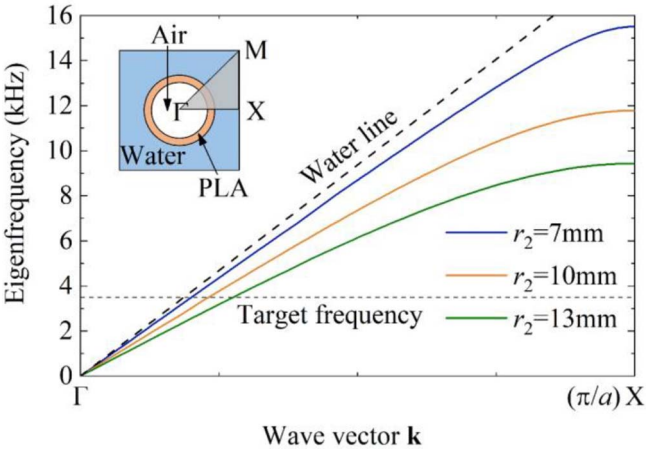

Figure 1. Band structures in $\Gamma - X$ direction of the PLA-Air phononic crystals with different scatterer's radii, $r_2 = 7$, 10 and 13 mm.

2 Luneburg lens based on phononic crystals

The Luneburg lens is designed by a discrete refraction-index profile using the GRIN phononic crystals [33]. In this work, the unit cell is composed of PLA (polylactic acid) and air inclusion in the water, as the inset picture illustrated in Figure 1. The PLA annulus is a commonly used 3D-printed material [23] whose Young's modulus, density and Poisson's ratio are $E = 3.2$ Gpa, $\rho = 1250$ kg/m^3 and $\mu = 0.3$, respectively. The density and sound speed of air are 1.205 kg/m^3 and 343 m/s, and those of water are 1025 kg/m^3 and 1500 m/s. As depicted in Figure 3, the inner and outer radii of the PLA annulus are r_1 and r_2 respectively, and the lattice constant is $a = 4$ cm. Return to Figure 1, the shaded area in the inset picture is the reduced Brillouin zone of phononic crystal with high symmetry points Γ, X, and M. The solid lines are the first energy band of longitudinal waves with respect to $r_2 = 7$, 10, and 13 mm. The band structure is calculated by COMSOL Multiphysics 5.5, including the acoustic module and mechanical module with an acoustic-solid coupling connection. The straight dashed black line is the energy band of water which indicates that the traveling waves don't have any dispersion during propagation. There are many references [34, 35] and websites[1,2] where readers can download the examples, available to calculate the band structure based on the Bloch-Floquet theory, so the detailed process of calculation is not given in this paper.

The target frequency for wave focusing is 3500 Hz. Figure 1 shows that the three energy bands are approximately straight lines around 3500 Hz. Therefore, the phase velocity which is nearly equal to the group velocity [17, 24, 36] can be directly calculated by $v_p = 2\pi f/k$ along the $\Gamma - X$ direction, where k is the reciprocal wavenumber. The effective refractive index is defined as $n_{eff} = v_w/v_p$, where v_w is the sound velocity in water. Compared with the steel inclusion whose radius is equal to r_2, the PLA-Air unit cell has a higher effective refraction index, as demonstrated in Figure 2a, so PLA-Air inclusion is a better choice for designing acoustic lens in water. The red points are the selected refraction indexes for designing the Luneburg lens.

The refraction-index profile of the Luneburg lens is $n = \sqrt{2 - r^2/R^2}$, where r is the distance from center, and $R = 0.32$ m is the radius of Luneburg lens in this work. As shown in Figure 2b, the black line is the ideal refraction index profile of the Luneburg lens, but a material satisfying the ideal refraction index profile doesn't exist in nature. Therefore, the refraction index profile is discretized as the red dashed line depicted in Figure 2b. Then a discretized Luneburg lens can be designed by finding matched unit cells in Figure 2a. Figure 3 demonstrated the acoustic Luneburg lens which is designed based on the refraction-index profile, and the number of unit cells is 177. The orange, blue and white parts are PLA, water and air, respectively.

3 Underwater sound direction identification

The difference between the Luneburg lens and other metalenses [5, 37, 38] is that the acoustic wave focusing can be achieved even though the acoustic wave comes from 360° directions, so it can be used to recognize the propagating direction of a sound wave. Figures 4a–4d presents the intensity field of focusing beam when a plane wave comes from the left side. The incident angles between the plane wave direction and x-axis are $\theta_i = 0°$, 15°, 30° and 45°, and $\theta_i = 0°$–45° is decided to be studied because the phononic-crystal Luneburg lens is a symmetry structure which can be divided into 8 parts. In the four cases, the maximum mesh size doesn't exceed 1/10 wavelength. To eliminate the wave reflection on the boundary of computational domain, the PML (perfectly matched layer) and wave radiation boundary are set around the whole region to simulate an

[1] https://www.comsol.com/blogs/modeling-phononic-band-gap-materials-and-structures
[2] https://www.comsol.de/model/sonic-crystal-16925

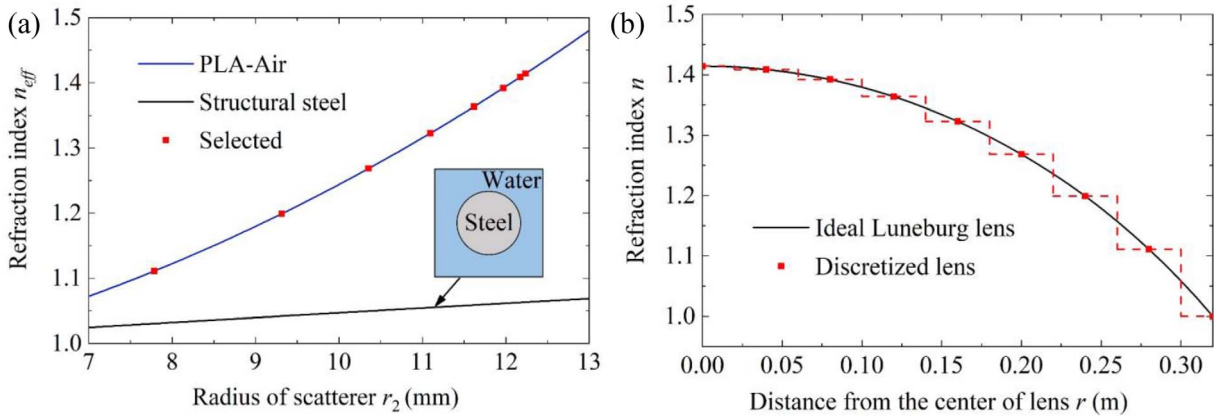

Figure 2. (a) Effective refraction index as a function of scatterer's radius. (b) Ideal and discretized refraction-index profile of Luneburg lens.

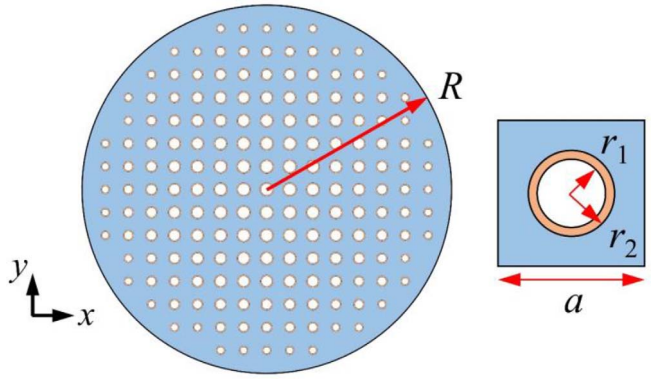

Figure 3. Acoustic Luneburg lens designed by square lattice and its unit cell.

infinite area. The incident pressure amplitude is 1 Pa which is applied by a background pressure field on water area. The interfaces between PLA and water, including PLA and air, are connected by an acoustic-structure coupling boundary. These simulations are carried out in the frequency domain. The results show that the designed Luneburg lens has the functionality of acoustic wave focusing, and the focusing beam is always on the opposite side of the incident plane.

The wave intensity corresponding to the four cases in Figures 4a–4d is extracted at $r = R + 0.04$ m (solid circle) where the total number of mesh elements is 1600. As shown in Figure 5a, the directivity of the focusing beams simultaneously varies with the incident angles. It implies that the sound direction can be directly detected by measuring the position of maximum intensity. In Figures 4a–4d and 5a, the angles between the focusing beam and x-axis are 0°, 14.93°, 30.15° and 45°. The focusing angles, 0° and 45°, are exact because the square-lattice Luneburg lens is symmetric at 0° and 45°. However, the focusing angles, 14.93° and 30.15°, are not accurate enough. The error can be contributed to that the discretized lens is not a complete circular lens with configuration defect. In order to improve the accuracy, as demonstrated in Figure 4e, the Luneburg lens is rotated according to the first measured angles ($\theta_a = 14.93°$ and 30.15°), and then the focusing angles are measured again. The secondly measured focusing angles are $\theta_b = 15.01°$ and 30°. This correction treatment obviously improves the precision of recognizing the sound direction, because the rotation correction procedure avoids the configuration defect for some incident angles. In practice, the hydrophone for measuring the maximum intensity can be installed on the symmetry axis of the Luneburg lens and rotated together with the Luneburg lens.

In this work, the designed frequency is 3500 Hz, but the acoustic wave focusing doesn't fail immediately when the working frequency isn't equal to the designed frequency. Hence, the bandwidth of acoustic wave focusing is studied. The focusing effect will disappear when the wavelength is much bigger than the size of Luneburg lens. In ultra-low frequency, due to acoustic wave diffraction, the wave can directly pass through the Luneburg lens. On the contrary, when the wavelength is much smaller than the size of Luneburg lens, irregular multiple scattering caused by unit cells will occur inside the phononic-crystal lens and generate band gaps. In order to study the bandwidth of the designed Luneburg lens, frequency from 1500Hz to 7500 Hz is simulated. Figure 5b is a directivity graph when the frequency is from 1500 Hz to 7500 Hz. The results suggest that the Luneburg has a narrow focusing beam and a broad range of working frequency for sound amplification. The focused intensity becomes higher when the frequency increases. In higher frequency, the wavelength is shorter, which leads more energy into the Luneburg lens while the size of Luneburg lens is unchanged. Moreover, as the frequency increases, the slope of the energy band in Figure 1 gradually becomes flat, so the effective velocity $v_p = 2\pi f/k$ is smaller. Then the effective refraction index of phononic crystal relative to water, $n_{\text{eff}} = v_w/v_p$, is greater. It also causes higher focused intensity when the frequency increases.

Furthermore, Table 1 provides the numerical results of sound direction identification for random incident angles with a frequency range of 1500–7500 Hz. The error is defined as $\xi = (X_2 - X_1)/1° \times 100\%$, where X_2 and X_1 are the numerical results and true value respectively. In this table, the biggest error of the first focusing angle θ_a is

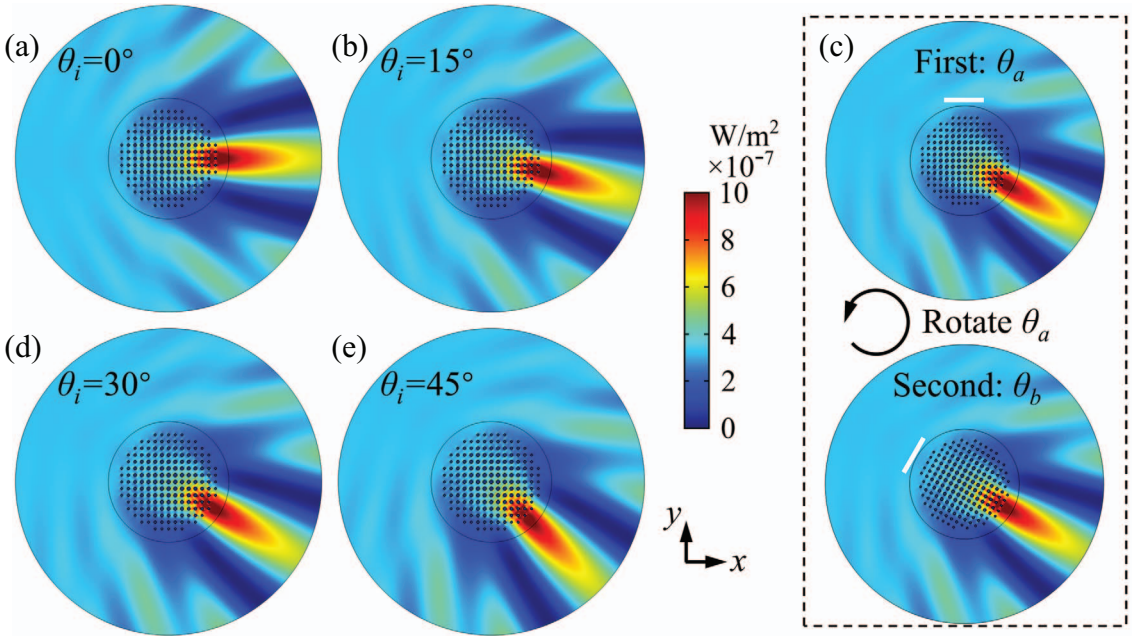

Figure 4. (a)–(d) Wave intensity field of acoustic wave focusing when the incident angles θ_i are 0°, 15°, 30° and 45°. (e) Rotation correction procedure of square-lattice Luneburg lens.

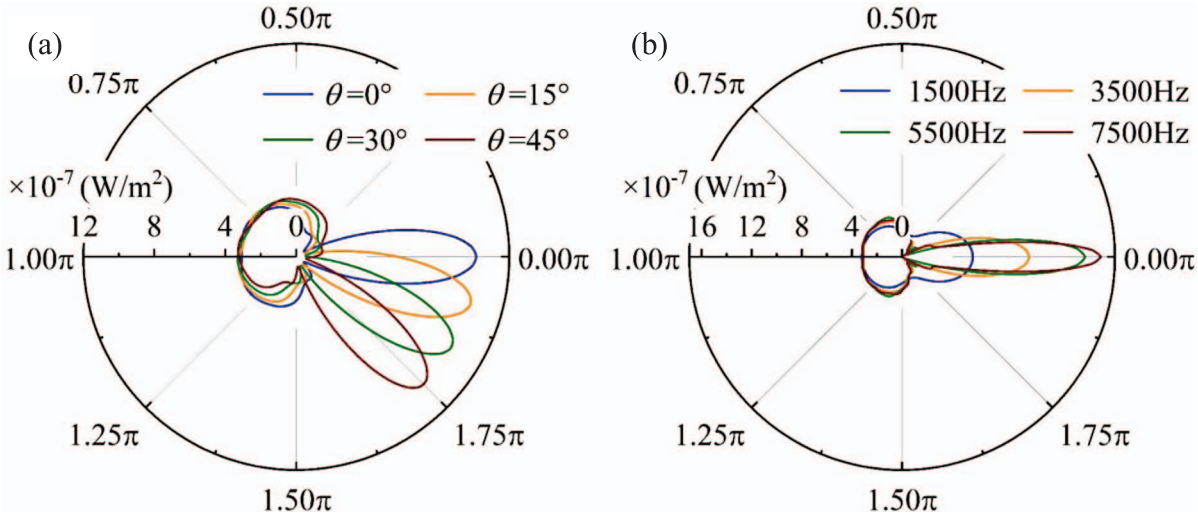

Figure 5. Wave intensity of acoustic wave focusing beam with different incident angles (a) and frequencies (b).

0.3° (ξ_1 = 30%), and the smallest error of θ_a is 0.08° (ξ_1 = 8%). By the rotation correction procedure in Figure 4e, the maximum angle error is reduced to 0.05° (ξ_2 = 5%), and the minimum error is decreased to 0° (ξ_2 = 0%). The accuracy of wave direction recognition is raised utilizing the symmetry axis of the square-lattice Luneburg lens. The rotation operation makes the symmetry axis approximately parallel to the direction of incident wave at different incident angles as much as possible. At the symmetry axis, the errors of direction identification are close to zero such as θ_i = 0° and 45° in Figure 4. In addition, compared with the traditional way (hydrophone array) to measure the sound direction, the Luneburg lens has a higher ratio of signal to noise because it can converge wave energy.

The phononic-crystal Luneburg lens can be designed to be of different sizes. Figure 6a shows the focusing intensity with different radii of the Luneburg lens, R = 0.32–0.64 m. It can be concluded that the focused intensity steadily increases when the radius of lens has an increase because the Luneburg lens with a larger radius has a wider receiving area for the incident wave, and the size of the acoustic lens doesn't have much influence on the relative width of focusing beam. In Figure 6b, the sound pressure level, SPL (dB) = 20 log($P_{\mathrm{rms}}/P_{\mathrm{ref}}$), as the function of frequency is analyzed. The root-mean-square pressure and the reference pressure in water are denoted by P_{rms} and P_{ref} = 1 μPa, respectively. The background sound pressure level is 116.99 dB when the incident pressure is 1 Pa. All the results

Table 1. Sound propagating direction identification with rotation correction.

Frequency f (Hz)	Incident angle θ_i (degree)	Focusing angle θ_a	Focusing angle θ_b	Errors ξ_1 (%)	Errors ξ_2 (%)
1500	15°	14.78°	15.00°	22	0
1500	30°	30.30°	30.00°	30	0
3500	20°	19.80°	20.03°	20	3
5500	5°	5.17°	4.95°	17	5
5500	42°	42.08°	42.00°	8	0
6500	37°	36.90°	36.99°	10	1
7500	11°	11.25°	11.03°	25	3

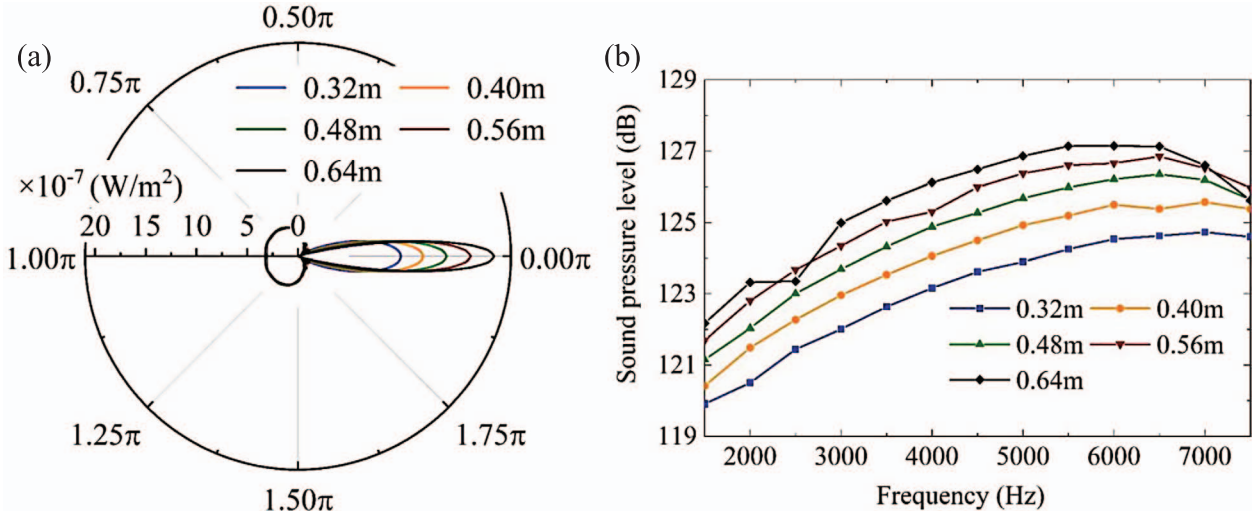

Figure 6. (a) Wave intensity of the acoustic wave focusing with different radii R of the Luneburg lens. (b) Sound pressure level as a function of frequency when the radius R is from 0.32 m to 0.64 m.

are bigger than the background sound pressure level due to the acoustic wave focusing. With the increase of frequency, the sound amplification level is higher, but the SPL begins going down after around 6500 Hz because the frequency is close to the bandgap [39] that a frequency band of the acoustic wave is forbidden propagating in the periodic structure. In this work, the bandgap of the longitudinal wave is above the first energy band. As shown in Figure 1, the starting frequency of the bandgap is near 9.43 kHz when the radius $r_2 = 13$ mm. If the working frequency exceeds 9.4 kHz into the bandgap, the phononic-crystal Luneburg lens will be disabled. In the first energy band, owing to the acoustic wave focusing, the Luneburg lens has the advantage of receiving a signal with intensity amplification to recognize the sound wave direction. Besides, it can use only one hydrophone or piezoelectric film around the lens to determine the direction of arbitrary incidence by measuring the position of maximum intensity, which would reduce the complexity of computation and integrated circuit than current positioning systems.

4 Underwater sound source localization

As a result of the direction identification, an unknown sound source can be detected through the triangulation location. In the far field, the wavefront of spherical wave and cylindrical wave generated by a point source can be regarded as a plane wave, so the wave energy can also be converged, which has been proved by experiments in our previous work [25]. As illustrated in Figure 7, the localization of the underwater object can be divided into three steps: firstly, measure the sound direction as the correction method described in the third section, and assume that the first measured direction is y-axis; secondly, perpendicularly move the Luneburg lens by d, and set the moving direction as x-axis; finally, measure another angle θ_2 and calculate the distance from the sound source to the center of Luneburg lens by $l_1 = d\tan(\theta_2)$. The first angle θ_1 is equal to 90° because the moving direction of the Luneburg lens is always perpendicular to the first measured direction. If the minimum angle which can be measured by sensors is 0.1° in reality, the distance l_1 is 35.80 m when $d = 1$ m and $\theta_2 = 88.4°$. The distance l_1 is 38.19 m when $d = 1$ m and $\theta_2 = 88.5°$. The deviation is (38.19–35.80)/38.19 = 6.26% that is greater than 5%. To guarantee the accuracy, the distance l_1 from 5 m to 35 m is studied as a short baseline positioning system in this work. The computation domain for sound localization is 4 × 2 m, and the sound source is applied by the background pressure field.

Table 2 compares the results of the underwater object localization with frequency from 1500 Hz to 7500 Hz. The movement of Luneburg lens d is 1 m, and the real distance is $l = 10$ m. From this table, the localization of the sound

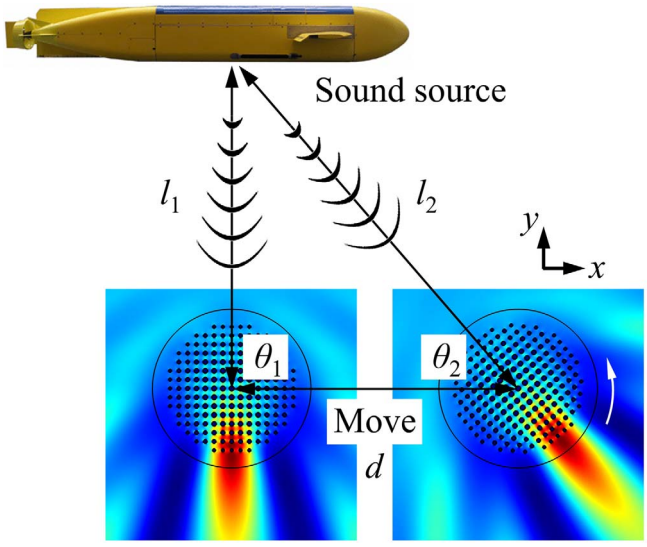

Figure 7. Schematic view of the underwater sound source localization.

source has a minimum error of 0.19% when the frequency is around the central frequency of 3500 Hz. Moreover, the real distance with a range of 5–35 m is given in Table 3. It shows that the errors have a growth when the distance of sound source increases. Some cases in Tables 2 and 3 are not precise enough, more than 1.00%, when the working frequency is off the designed frequency 3500 Hz or the distance of sound source increases. Hence, to improve the localization precision, we change the movement d from 1.5 m to 2.5 m, as listed in Table 4. From the first three rows, it can be seen that the measurements become more accurate with the increase of the movement d. The errors are reduced from 1.74% to 0.19% in the case of $f = 3500$ Hz and $d = 2.5$ m. About the cases of 1500 Hz and 7500 Hz in the Table 2, the errors are decreased to 0.64% by setting $d = 2.5$ as shown in Table 4. Therefore, by means of the triangulation location, the designed Luneburg lens can be used to search for an unknown sound source within 35 m precisely.

5 Phononic-crystal Luneburg lens by annular lattice

However, we always worry about the phononic-crystal Luneburg lens's unsmooth outline that may bring about a greater discrepancy when the source direction and position are unknown. As the results are shown in Table 1, the approximatively circular shape by square lattice reduces the reliability of sensitive directivity, and the rotation correction procedure for sound direction recognition and localization is really clumsy and slow. In addition, the Luneburg lens designed by square lattice costs a lot of time for geometry modeling. As sketched in Figure 8a, the Luneburg lens with square lattice needs to arrange the unit cell one by one in the 1/8 symmetry model, because the radii of unit cells

Table 2. Underwater sound localization when the frequency f is 1500–7500 Hz.

Frequency f (Hz)	Movement d (m)	Real distance l (m)	Numerical results l_1	Errors ξ_2 (%)
1500	1	10	10.153	1.53
2500	1	10	10.153	1.53
3500	1	10	10.019	0.19
4500	1	10	10.019	0.19
5500	1	10	10.019	0.19
6500	1	10	10.153	1.53
7500	1	10	10.153	1.53

are different from center to border of the Luneburg lens. If the radius of Luneburg lens is bigger, it will take more time for geometry modeling. For example, when the radius of Luneburg lens is $R = 0.64$ m, the total number of cylinders is 751 which leads the geometry modeling to be a time-consuming task. Inspired by Maxwell's fish-eye lens which is composed of annular arrays [9], in this section, an alternative method is proposed to design the Luneburg lens. It will save a lot of time to design the Luneburg lens, and the focusing wave is more isotropy for sound direction recognition and positioning. Figure 8b shows the Luneburg lens with an annular arrangement of phononic crystals. The geometry modeling of annular-lattice Luneburg lens just needs a rotation array at each radius. There are Round $[2\pi r/a]$ cylinders at each radius r, and the total number of unit cells is equal to the squarely arranged one in Figure 8a, so this kind of design doesn't increase the material consumption. Different from the square lattice, the annular-lattice Luneburg lens with rotation array doesn't need to align the unit cell one by one, which significantly simplifies the geometric modeling. Figure 9 demonstrates the focusing beam of the second Luneburg lens. Compared with the intensity field in Figure 4, it means that the redesigned Luneburg doesn't change the focusing effect.

To further verify the functionality of the second Luneburg lens, the wave focusing beam, frequency response of sound pressure level and lens size are all analyzed. As shown in Figure 10a, the black and red lines are the intensity distribution along the arc at $r = 0.36$ m concerning the Luneburg lenses with square and annular lattice. Two solid lines show a small discrepancy when the incident angle θ_i is 0° where wave direction parallels the symmetry axis of square-lattice Luneburg lens. It implies that the annular-lattice Luneburg lens doesn't change the focusing property based on GRIN phononic crystal. For the annular-lattice Luneburg lens, the intensity distribution with incident angles $\theta_i = 3°$, 14°, 22°, and 41° are also calculated in Figure 10b. The focusing angles of these four cases are 3°, 14.03°, 22.05°, and 40.95°, respectively. The errors of sound direction recognition don't exceed 5%, so the accuracy is better than the focusing angle that is directly calculated by the square-lattice Luneburg lens, as ξ_1 (8–30%) demonstrated in Table 1. The annular-lattice Luneburg lens has smaller errors than the square-lattice one, because the annular-lattice one is more isotropic for incident waves. If the width of focusing beam is defined as the interval

Table 3. Underwater sound localization when the distance l is 5 – 35 m.

Frequency f (Hz)	Movement d (m)	Real distance l (m)	Numerical results l_1	Errors ξ_2 (%)
3500	1	5	5.027	0.54
3500	1	15	14.957	0.29
3500	1	20	20.088	0.44
3500	1	25	25.452	1.81
3500	1	30	30.548	1.83
3500	1	35	36.369	3.91

Table 4. Underwater sound localization when movement d is 1.5 – 2.5 m.

Frequency f (Hz)	Movement d (m)	Real distance l (m)	Numerical results l_1	Errors ξ_2 (%)
3500	1.5	25	25.435	1.74
3500	2.0	25	25.412	1.65
3500	2.5	25	25.047	0.19
3500	2.5	35	35.309	0.88
1500	2.5	10	10.064	0.64
7500	2.5	10	10.064	0.64

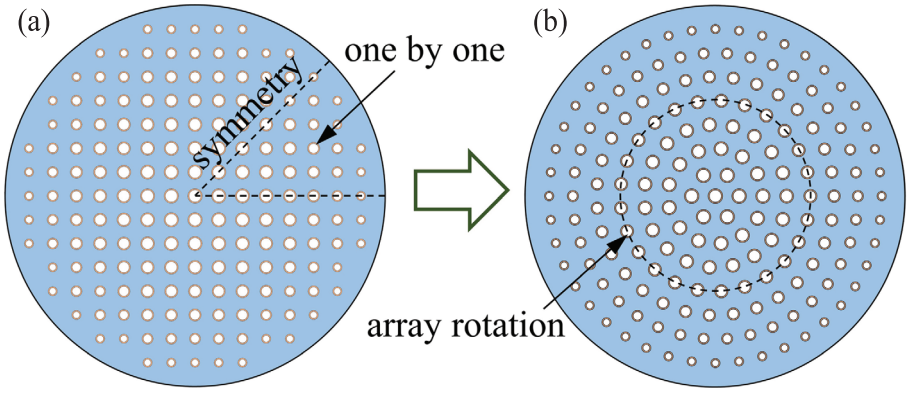

Figure 8. (a) Luneburg lens designed by square lattice. (b) Luneburg lens designed by annular lattice.

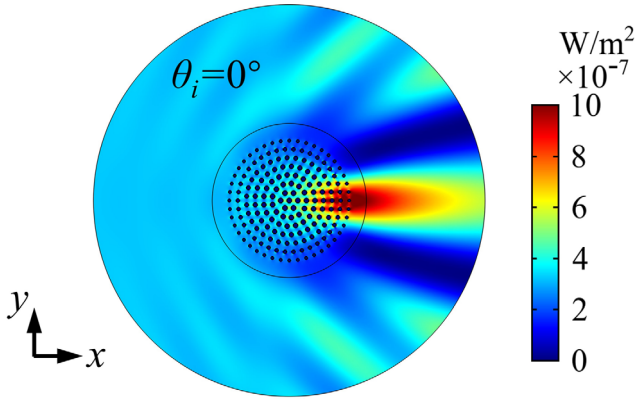

Figure 9. Wave intensity field of the Luneburg lens with an annular arrangement.

between positions at $I_{\max}/\sqrt{2}$, where $I_{\max}$ is the maximum intensity. In the four cases, the largest width is 23.85°, and the smallest width is 23.78°. The width of focusing beam has little fluctuation when the incident angle changes, so the annular-lattice Luneburg lens can be regarded as a nearly isotropic lens for incident waves. Figure 10c is the sound pressure level as a function of frequency. The sound pressure level is extracted from the focusing intensity at $r = 0.36$ m too. It shows that the annular-lattice Luneburg lens has a similar frequency response to the square-lattice Luneburg lens. Furthermore, the annular-lattice one also doesn't change the focusing effect when the lens size is redesigned as demonstrated in Figure 10d. Therefore, all the results indicate that the redesigned Luneburg lens with annular arrays has little impact on the focusing effect, but the annular arrays make the configuration more isotropy.

The redesigned Luneburg lens can improve the accuracy of sound localization because it is nearly isotropic for any incident angles. To clearly illustrate the advantages of annular-lattice Luneburg lens, an example is demonstrated in Figure 11. The incident angle and the working frequency are 5° and 5500 Hz respectively. The solid lines in the picture are the wave intensity of focusing beams, and the dashed lines are drawn at the peak intensity with respect to square lattice and annular lattice. After the sound wave

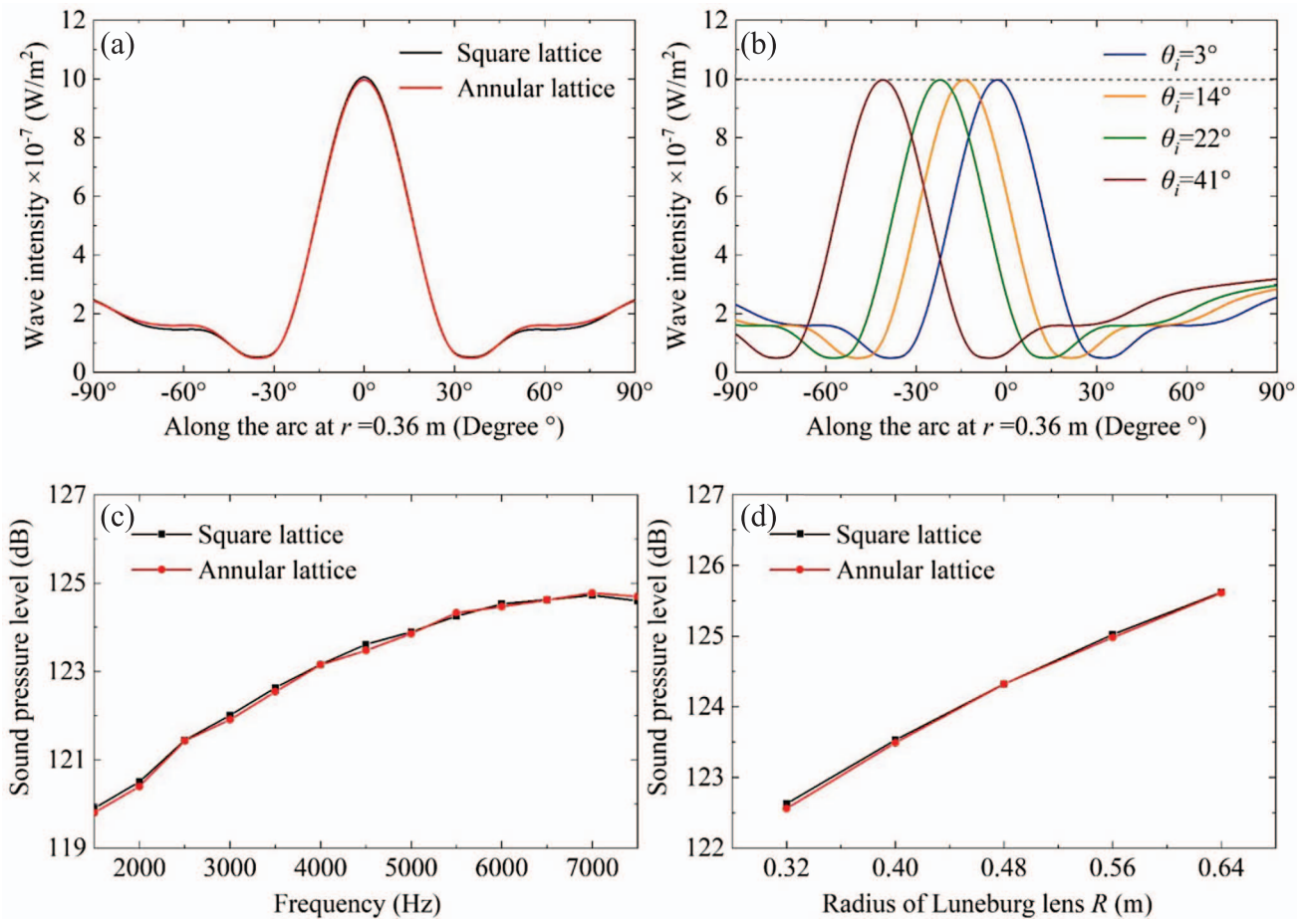

Figure 10. (a) Wave intensity along the arc when $r = 0.36$ m when $\theta_i = 0°$. (b) Wave intensity profile when $\theta_i = 3°$, 14°, 22°, 41°, respectively. (c) Sound pressure level as a function of frequency. (d) Sound pressure level with the radius of Luneburg lens increased.

converges, the acquired focusing angle of square-lattice Luneburg lens is 5.17°, and the error of focusing angle is 17%. By comparison, the focusing angle of annular-lattice Luneburg lens is 4.95°, and the error is only $5 < 17\%$. Besides the example, in our simulation, the accuracy of annular lattice is all higher than the square lattice without rotation correction procedure in Figure 4e. Only the lattice form is changed in these cases, so we think the error is caused by the configuration defect of square-lattice Luneburg lens. As listed in Table 5, the symbols ξ_1, ξ_2 and ξ_3 represent the errors of square-lattice Luneburg lens without rotation correction procedure, square-lattice one with rotation correction procedure and annular-lattice one without rotation correction procedure, respectively. The computation domain and mesh elements for sound localization simulation are consistent with the cases in the third section. The square-lattice one without rotation correction procedure has the worst precision because of the configuration defect. The largest error is 9.42%, and the smallest value is 4.56%. The square-lattice one with rotation correction procedure makes the accuracy better. The largest error is 3.91%, and the smallest value is 1.53%. However, the rotation measurements are clumsy and slow. By calculating the annular-lattice Luneburg lens which doesn't need a rotation correction procedure, the largest error is 2.09%, and the smallest error is only 0.02%. Better results are obtained by the redesigned Luneburg lens. Therefore, making a comparison of geometrical modeling

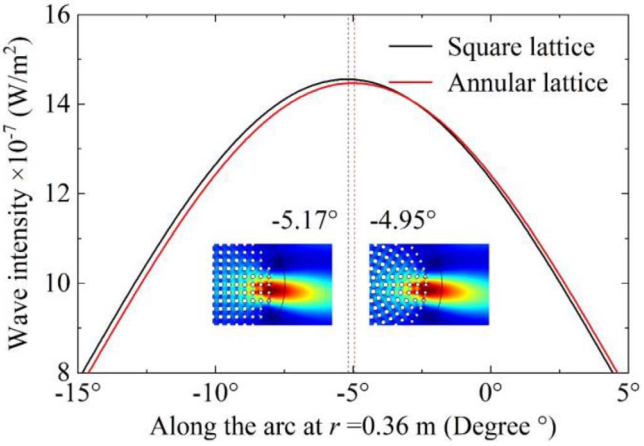

Figure 11. The focusing angles of square-lattice and annular-lattice Luneburg lens when the incident angle and frequency are 5° and 5500 Hz, respectively.

Table 5. The errors of rearranged Luneburg lens for sound localization.

Frequency f (Hz)	Movement d (m)	Real distance l (m)	Errors ξ_1 (%)	Errors ξ_2 (%)	Errors ξ_3 (%)
3500	1	25	4.56	1.81	1.81
3500	1	30	5.73	1.83	2.09
3500	1	35	5.13	3.91	0.81
1500	1	10	6.04	1.53	1.53
7500	1	10	9.42	1.53	1.53
3500	1.5	25	4.63	1.74	1.74
3500	2.0	25	4.73	1.65	0.02

and accuracy, the annular-arranged Luneburg lens is more applicable than the square-lattice one obviously.

6 Conclusions

In conclusion, we designed a phononic-crystal Luneburg lens in a water environment which can be used to recognize wave direction and locate a sound source with sound amplification. The numerical results show that the Luneburg lens has a high accuracy of direction identification for 360° incident angles with a broadband frequency range between 1500 Hz and 7500 Hz. Meanwhile, the acoustic wave focusing improves the signal-to-noise ratio, so it enables only one hydrophone to be used for sound direction recognition and locating the position of an unknown sound source from 5 m to 35 m, with errors below 1% by increasing the movement d properly. To improve the functionality and reliability, a Luneburg lens composed of annular lattices is redesigned based on the gradient phononic crystals. The comparison results show that the annular-lattice Luneburg lens not only guarantees accuracy but also reduces complexity for geometric modeling. The phononic-crystal Luneburg lens may have an application prospect of next-generation sonar in underwater technology, such as underwater acoustic positioning systems and acoustic wireless communication [13, 19, 40]. In future, multiple sources, 3D detecting, moving targets and a silent object may also be developed. In addition, the experimental validation also needs to be carried out for further application.

Data availability

The data and programs that support the findings of this study are available from the corresponding author upon reasonable request.

Acknowledgments

This work was supported in part by the National Natural Science Foundation of China (Grant Nos. 51879231 and 51679214), the High-tech Ship Research Project of the Ministry of Industry and Information Technology, the Primary Research and Development Plan of Zhejiang Province (Grant Nos. 2019C03115 and 2019C02050), the Zhejiang Daishan No. 4 Project of China General Nuclear Power Group, the Marine Innovation and Development Demonstration Project of State Oceanography Bureau (Grant No. PD-HY-002). Ruan thanks Chuanjie Hu from Xiamen University for the helpful discussion.

Conflict of interest

The authors have no conflicts to disclose.

References

1. Y. Zhang, K. Chen, X. Hao, Y. Cheng: A review of underwater acoustic metamaterials. Kexue Tongbao/Chinese Science Bulletin 65, 15 (2020) 1396–1410.
2. S. Huang, L. Peng, H. Sun, Q. Wang, W. Zhao, S. Wang: Frequency response of an underwater acoustic focusing composite lens. Applied Acoustics 173 (2021) 107692.
3. M. Duan, C. Yu, F. Xin, T.J. Lu: Tunable underwater acoustic metamaterials via quasi-Helmholtz resonance: From low-frequency to ultra-broadband. Applied Physics Letters 118, 7 (2021) 071904.
4. Y. Shen, C. Qiu, X. Cai, L. Ye, J. Lu, M. Ke, Z. Liu: Valley-projected edge modes observed in underwater sonic crystals. Applied Physics Letters 114, 2 (2019) 023501.
5. J. Chen, J. Rao, D. Lisevych, Z. Fan: Broadband ultrasonic focusing in water with an ultra-compact metasurface lens. Applied Physics Letters 114, 10 (2019) 104101.
6. A. Sukhovich, L. Jing, J.H. Page: Negative refraction and focusing of ultrasound in two-dimensional phononic crystals. Physical Review B 77, 1 (2008) 014301.
7. L. Wu, L. Chen: An acoustic bending waveguide designed by graded sonic crystals. Journal of Applied Physics 110, 11 (2011) 114507.
8. B. Li, J. Guan, K. Deng, H. Zhao: Splitting of self-collimated beams in two-dimensional sonic crystals. Journal of Applied Physics 112, 12 (2012) 124514.
9. B. Yuan, Y. Tian, Y. Cheng, X. Liu: An acoustic Maxwell's fish-eye lens based on gradient-index metamaterials. Chinese Physics B 25, 10 (2016) 104301.
10. X. Hu, C.T. Chan, J. Zi: Two-dimensional sonic crystals with Helmholtz resonators. Physical Review E 71, 5 (2005) 055601.
11. S.S. Lin, B.R. Tittmann, T.J. Huang: Design of acoustic beam aperture modifier using gradient-index phononic crystals. Journal of Applied Physics 111, 12 (2012) 123510.
12. Y. Xie, Y. Fu, Z. Jia, J. Li, C. Shen, Y. Xu, H. Chen, S.A. Cummer: Acoustic imaging with metamaterial Luneburg lenses. Scientific Reports 8, 1 (2018) 16188.
13. S. Kim: Sound focusing by acoustic Luneburg lens (2014). ArXiv preprint [arXiv: 1409.5489]

14. Y. Fu, J. Li, Y. Xie, C. Shen, Y. Xu, H. Chen, S.A. Cummer: Compact acoustic retroreflector based on a mirrored Luneburg lens. Physical Review Materials 2, 10 (2018) 105202.
15. S. Tol, F.L. Degertekin, A. Erturk: Phononic crystal Luneburg lens for omnidirectional elastic wave focusing and energy harvesting. Applied Physics Letters 111, 1 (2017) 013503.
16. N.J. Whitehead, S.A.R. Horsley, T.G. Philbin, V.V. Kruglyak: A Luneburg lens for spin waves. Applied Physics Letters 113, 21 (2018) 212404.
17. S.S. Lin, T.J. Huang, J. Sun, T. Wu: Gradient-index phononic crystals. Physical Review B 79, 9 (2009) 094302.
18. J. Kim, S. Lee, J. Jo, S. Wang, S. Kim: Acoustic imaging by three-dimensional acoustic Luneburg meta-lens with lattice columns. Applied Physics Letters 118, 9 (2021) 091902.
19. S. Kim, Byeong-Won, Kyung-Min, G.S. Lim: Sound reception system by an acoustic Luneburg lens (2019). ArXiv preprint [arXiv: 1906.07174]
20. C.M. Park, S.H. Lee: Acoustic Luneburg lens using orifice-type metamaterial unit cells. Applied Physics Letters 112, 7 (2018) 074101.
21. L. Zhao, E. Laredo, O. Ryan, A. Yazdkhasti, H. Kim, R. Ganye, T. Horiuchi, M. Yu: Ultrasound beam steering with flattened acoustic metamaterial Luneburg lens. Applied Physics Letters 116, 7 (2020) 071902.
22. R. Yu, H. Wang, W. Chen, C. Zhu, D. Wu: Latticed underwater acoustic Luneburg lens. Applied Physics Express 13, 8 (2020) 84003.
23. A. Allam, K. Sabra, A. Erturk: 3D-printed gradient-index phononic crystal lens for underwater acoustic wave focusing, Physical Review Applied 13, 6 (2020) 064064.
24. C. Lu, R. Yu, Q. Ma, K. Wang, J. Wang, D. Wu: GRIN metamaterial generalized Luneburg lens for ultra-long acoustic jet. Applied Physics Letters 118, 14 (2021) 144103.
25. Y. Ruan, X. Liang, Z. Wang, T. Wang, Y. Deng, F. Qu, J. Zhang: 3-D underwater acoustic wave focusing by periodic structure. Applied Physics Letters 114, 8 (2019) 081908.
26. H. Sun, S. Wang, S. Huang, L. Peng, Q. Wang, W. Zhao, J. Zou: 3D focusing acoustic lens optimization method using multi-factor and multi-level orthogonal test designing theory. Applied Acoustics 170 (2020) 107538.
27. H. Sun, S. Wang, S. Huang, L. Peng, Q. Wang, W. Zhao: Design and characterization of an acoustic composite lens with high-intensity and directionally controllable focusing. Scientific Reports 10, 1 (2020) 1469.
28. H.C. Song, G. Byun: Localization of a distant ship using a guide ship and a vertical array. The Journal of the Acoustical Society of America 149, 4 (2021) 2173–2178.
29. H.C. Song, C. Cho: Array invariant-based source localization in shallow water using a sparse vertical array. The Journal of the Acoustical Society of America 141, 1 (2017) 183–188.
30. M. Brandstein: Microphone arrays: Signal processing techniques and applications. Springer Science & Business Media, Germany, 2001.
31. J. Gu, W. Lin, C. Kan: Sound source localization using piezoelectric acoustic metasurfaces. Acoustics Australia 48, 3 (2020) 455–461.
32. X. Sun, H. Jia, Z. Zhang, Y. Yang, Z. Sun, J. Yang: Sound localization and separation in 3D space using a single microphone with a metamaterial enclosure. Advanced Science 7, 3 (2020) 1902271.
33. Y. Jin, B. Djafari-Rouhani, D. Torrent: Gradient index phononic crystals and metamaterials. Nanophotonics 8, 5 (2019) 685–701.
34. Y. Cao, Z. Hou, Y. Liu: Finite difference time domain method for band-structure calculations of two-dimensional phononic crystals. Solid State Communications 132, 8 (2004) 539–543.
35. G. Wang, J. Wen, Y. Liu, X. Wen: Lumped-mass method for the study of band structure in two-dimensional phononic crystals. Physical Review B 69, 18 (2004) 184302.
36. Y. Tian, Z. Tan, X. Han, W. Li: Phononic crystal lens with an asymmetric scatterer. Journal of Physics D: Applied Physics 52, 2 (2019) 25102.
37. D.C. Calvo, A.L. Thangawng, M. Nicholas, C.N. Layman: Thin Fresnel zone plate lenses for focusing underwater sound. Applied Physics Letters 107, 1 (2015) 014103.
38. D. Tarrazó-Serrano, S. Pérez-López, P. Candelas, A. Uris, C. Rubio: Acoustic focusing enhancement in Fresnel Zone Plate Lenses. Scientific Reports 9, 1 (2019) 7067.
39. Y. Pennec, J.O. Vasseur, B. Djafari-Rouhani, L. Dobrzyński, P. A. Deymier: Two-dimensional phononic crystals: Examples and applications. Surface Science Reports 65, 8 (2010) 229–291.
40. X. Su, I. Ullah, X. Liu, D. Choi: A review of underwater localization techniques, algorithms, and challenges. Journal of Sensors 2020 (2020) 6403161.

Cite this article as: Ruan Y. & Liang X. 2022. 2D phononic-crystal Luneburg lens for all-angle underwater sound localization. Acta Acustica, **6**, 12.